Structure and Vibrational Spectra of Chlorofluorocarbon Substitutes: An Experimental and ab Initio Study of Fluorinated Ethers CHF_2OCF_3 (E125), CHF_2OCHF_2 (E134), and CH_3OCF_3 (E143A)

D. A. Good and J. S. Francisco*

Department of Chemistry and Department of Earth & Atmospheric Sciences, Purdue University, West Lafayette, Indiana 47907-1393

Received: October 31, 1997; In Final Form: January 5, 1998

The fundamental IR vibrational modes of CHF_2OCF_3 (E125), CHF_2OCHF_2 (E134), and CH_3OCF_3 (E143a) have been examined by ab initio molecular orbital calculations and have been compared with FT-IR measurements. A complete assignment of all fundamental vibrational modes has been made for each fluorinated ether. As a calibration for the fluorinated ethers, the fundamental IR vibrational modes of dimethyl ether have been reexamined by ab initio methods and have been compared with literature assignments.

I. Introduction

Since recognizing the chlorofluorocarbon's (CFCs) deleterious effects on ozone, the scientific and engineering communities have sought replacements for these extraordinarily stable molecules. The development of new alternatives has centered around the reduction or elimination of chlorine and the addition of hydrogen into the parent molecule. The elimination of chlorine would reduce the molecule's ozone depletion potential (ODP) to near zero, while the addition of hydrogen would allow the molecule to degrade in the troposphere as mediated by hydroxyl radical. The rate of this reaction with hydroxyl radical determines the molecule's atmospheric lifetime.

Partially fluorinated ethers have been proposed as potential chlorofluorocarbon replacements, not only because of their lack of chlorine and resulting low ODPs but also because of their suspected short atmospheric lifetimes, as compared to analogous hydrofluorocarbons (HFCs).[1−3] Cooper et al.[3] used semiempirical and SCF ab initio methods to compare the lifetimes of fluorinated ethers with their corresponding hydrofluorocarbons. In all cases but one (CF_3OCHF_2 vs CF_3CHF_2) the fluorinated ether was found to have a substantially shorter lifetime.[3]

Lifetime determinations are necessary for the evaluation of a molecule's ability to perturb the earth/atmosphere radiative balance, i.e., global warming potential (GWP). A second factor that is crucial to this determination is a knowledge of a molecule's ability to absorb and thus prevent longwave (infrared) radiation from escaping the atmosphere.[4] Information on where and how strongly a molecule absorbs infrared radiation is obtained through a determination of a molecule's vibrational spectra. To date, no information on the vibrational spectroscopy of partially fluorinated ethers has been reported in the literature. We present an investigation of the structural, rotational, and vibrational properties of partially fluorinated ethers CHF_2OCF_3 (E125), CHF_2OCHF_2 (E134), and CH_3OCF_3 (E143a).

II. Methods

All calculations were carried out using the GAUSSIAN 94 program.[5] All geometries were fully optimized with no constraints to better than 0.001 Å for bond lengths and 0.1° for angles. The geometries were optimized at the second-order Møller−Plesset perturbation (MP2)[6] and quadratic configuration interaction with single and double excitation (QCISD)[7] levels of theory. These optimizations were carried out with the medium size double-split valence basis set, 6-31G(d). Optimizations were also performed with the Becke nonlocal three-parameter exchange and correlation functional with the Lee−Yang−Parr correctional functional method (B3LYP) with the large 6-311++G(3df,3pd) basis set.[8] Vibrational frequencies were determined using MP2, QCISD, and B3LYP methods.

III. Results and Discussion

A. Structure of Fluorinated Ethers. Correlation between a molecule's structure and reactivity is useful in the development of empirical methods for the estimation of rate constants. Thus, a thorough knowledge of the structure of hydrofluorinated ethers may provide insights into their reactivity trends. DeMore et al.[2] and Kurylo et al.[1] have described substituent effects on hydroxyl radical reaction rates for fluorinated ethers. The addition of an ether linkage in ethane to form dimethyl ether results in an enhancement in the rate of reaction with hydroxyl radical by a factor 9.[1] Successive substitution of hydrogen for fluorine in dimethyl ether successively slows the reaction with hydroxyl radical.[2] A question we intend to address is how a molecule's structure changes from the basic dimethyl ether framework upon fluorination.

The structure of dimethyl ether, as determined using the above methodology, is illustrated and tabulated in Figure 1 and Table 1, respectively. Dimethyl ether was used as a calibrant in this investigation because its structure has been previously determined. Myers et al.[9] determined the structure of dimethyl ether from microwave experiments. Their first consideration assumed symmetric methyl groups with equivalent C−H distances. However, in their later study, dimethyl ether was identified as having two distinct hydrogen environments, a conclusion supported by our calculations.[10] In the Myers et al.[9] experiments, the structure was derived from analysis of rotational constants from six assigned isotopic derivatives of dimethyl ether. The experimental CC bond length derived from the microwave spectra is 1.410 ± 0.003 Å. Our predicted CC bond length at the MP2/6-31G(d) level is 1.414 Å and at the QCISD-

S1089-5639(98)00048-6 CCC: $15.00
Published on Web 02/12/1998

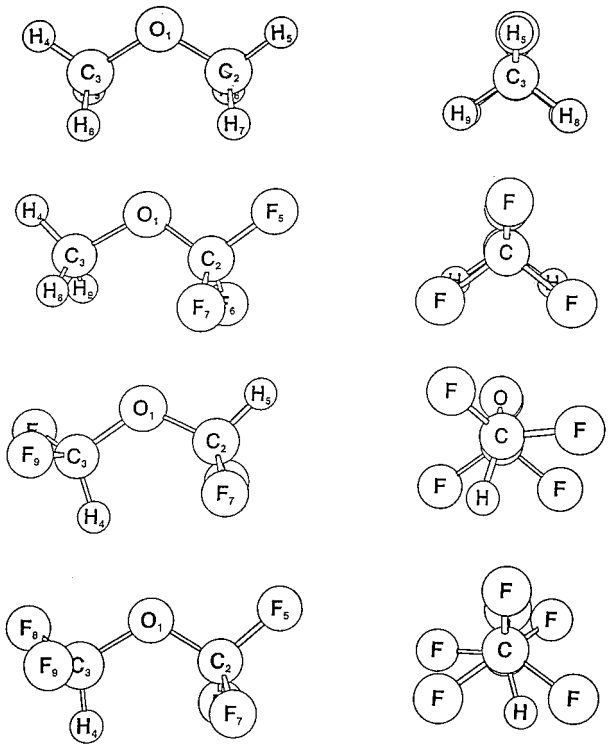

Figure 1. Optimized geometry labeling of dimethyl and fluorinated ethers. See Table 1 for detailed parameters.

(T)/6-31G(d) level is 1.416 Å. Both these predictions overestimate the CC bond length by 0.004 and 0.006 Å, respectively. Using the B3LYP/6-311++G(3df,3pd) level of theory, the CC bond length is predicted to be in excellent agreement with experiment.

The equatorial CH bonds are predicted to be 0.009 Å longer than the axial CH bonds at all levels of theory. This is confirmed by experiment, which reveals that the equatorial CH bonds are indeed 0.009 Å longer than the axial CH bonds.[9] We find that theory does a good job at estimating the equatorial CH bond lengths. At the highest level of theory, B3LYP/6-311++G(3df,3pd), the difference between predicted and experimental equatorial CH bond lengths is 0.003 Å. This is well within the experimental uncertainty limits of ±0.005 Å. Agreement in the predicted axial CH bond length is also reasonable. The rms deviation is 0.003 Å for the various levels of theory. The rms error between calculated and experimental bond angles is 0.5% at the B3LYP/6-311++G(3df,3pd) level. From the dimethyl ether results we find that the B3LYP/6-311++G(3df,3pd) level of theory predicts a reliable structure.

The substitution of three hydrogens for three fluorine atoms to form CH_3OCF_3 (E143a) does little to change the conformation from that of dimethyl ether. The molecule is still in an eclipsed geometry with a vertical plane traversing the length of the molecule yielding C_s symmetry. The electron-withdrawing nature of the CF_3 group imparts subtle changes from the dimethyl ether structure. The COC angle in dimethyl ether is smaller than the COC angle in E143a. This is due to oxygen−fluorine atom repulsions. There is no evidence for hydrogen bonding between hydrogen and fluorine in the equatorial position. The hydrogen (equatorial)−hydrogen (equatorial) distance (2.464 Å) in dimethyl ether is shorter than the hydrogen (equatorial)−fluorine (equatorial) distance (2.552 Å) in E143a.

TABLE 1: Optimized Geometries[a] of Fluorinated Ethers

	CH_3OCH_3				CH_3OCF_3 (E143a)			CHF_2OCHF_2 (E134)			CHF_2OCF_3 (E125)		
coordinate	MP2	QCISD	B3LYP	expt[b]	MP2	QCISD	B3LYP	MP2	QCISD	B3LYP	MP2	QCISD	B3LYP
$R(C_3X_4)$	1.090	1.094	1.088	1.091 ± 0.007	1.087	1.091	1.084	1.089	1.091	1.088	1.090	1.092	1.089
$R(C_3X_8)$	1.099	1.103	1.097	1.100 ± 0.005	1.091	1.094	1.088	1.346	1.347	1.343	1.343	1.342	1.338
$R(C_3X_9)$	1.099	1.103	1.097	1.100 ± 0.005	1.091	1.094	1.088	1.351	1.351	1.347	1.35	1.349	1.344
$R(C_2X_5)$	1.090	1.094	1.088	1.091 ± 0.007	1.333	1.333	1.329	1.087	1.089	1.086	1.327	1.325	1.321
$R(C_2X_6)$	1.099	1.103	1.097	1.100 ± 0.005	1.353	1.352	1.351	1.362	1.361	1.358	1.349	1.347	1.343
$R(C_2X_7)$	1.099	1.103	1.097	1.100 ± 0.005	1.353	1.352	1.351	1.359	1.359	1.356	1.345	1.343	1.340
$R(C_2O)$	1.414	1.416	1.410	1.410 ± 0.003	1.344	1.345	1.337	1.373	1.374	1.367	1.365	1.363	1.360
$R(C_3O)$	1.414	1.416	1.410	1.410 ± 0.003	1.440	1.442	1.439	1.392	1.392	1.388	1.399	1.397	1.395
X_4C_3O	106.9	107.0	107.4	107.2 ± 0.6	104.9	105.0	105.3	113.0	113.1	113.3	112.7	112.7	113.0
X_8C_3O	111.5	111.5	111.4	110.8 ± 0.3	110.3	110.3	110.5	106.7	106.8	107.6	105.9	106.0	106.8
X_9C_3O	111.5	111.5	111.4	110.8 ± 0.3	110.3	110.3	110.5	109.2	109.1	108.7	109.4	109.4	109.0
X_5C_2O	106.9	107.0	107.4	107.2 ± 0.6	108.3	108.3	108.6	108.3	108.4	108.3	107.8	107.8	107.8
X_6C_2O	111.5	111.5	111.4	110.8 ± 0.3	112.6	112.6	112.8	110.7	110.6	111.2	111.5	111.8	111.8
X_7C_2O	111.5	111.5	111.4	110.8 ± 0.3	112.6	112.6	112.8	110.9	110.8	111.4	111.9	111.9	112.2
COC	111.1	111.4	112.9	111.7	114.4	114.7	116.4	114.9	115.2	117.7	115.2	115.5	117.6
$X_4C_3OC_2$	180.0	180.0	180.0	180.0	180.0	180.0	180.0	22.1	19.8	10.4	30.9	30.8	19.5
$X_8C_3OC_2$	−60.7	−60.7	−60.7		−61.3	−61.2	−61.3	143.4	141.2	132.0	151.9	151.8	140.9
$X_9C_3OC_2$	60.7	60.7	60.7		61.3	61.2	61.3	−100.1	−102.4	−111.8	−91.3	−91.5	−102.7
$X_5C_2OC_3$	180.0	180.0	180.0	180.0	180.0	180.0	180.0	175.4	175.5	179.2	174.5	174.5	177.3
$X_6C_2OC_3$	60.7	60.7	60.7		−60.1	−60.1	−60.1	−63.9	−63.6	−60.1	−65.8	−65.9	−63.1
$X_7C_2OC_3$	−60.7	−60.7	−60.7		60.1	60.1	60.1	53.9	54.1	58.1	54.1	54.0	57.1

[a] Bond lengths in Å and bond angles in deg. [b] Blukis, U.; Kasai, P. H.; Myers, R. J. *J. Chem. Phys.* **1963**, *38*, 2753.

TABLE 2: Rotational Constants[a] for Dimethyl Ether and Fluorinated Ethers

	CH_3OCH_3			CH_3OCF_3			CHF_2OCHF_2			CHF_2OCF_3		
level of theory	*A*	*B*	*C*	*A*	*B*	*C*	*A*	*B*	*C*	*A*	*B*	*C*
MP2/6-31G(d)	38 550	10 113	8917	5387	3058	3032	4582	1930	1535	3685	1395	1257
QCISD/6-31G(d)	38 530	10 050	8875	5422	3039	3015	4612	1828	1497	3700	1373	1238
B3LYP/6-311++G(3df,3pd)	39 670	9 977	8865	5396	3051	3026	4576	1921	1528	3697	1395	1258
experiment[b]	38 788	10 056	8887									

[a] Rotational constants given in units of MHz. [b] Neustock, W.; Guarnieri, A.; Demaison, J.; Wlodarezak, G. *Naturforsch Z.* **1990**, *45a*, 702.

TABLE 3: Asymmetry Parameters

	level of theory		
species	MP2/ 6-31G(d)	QCISD/ 6-31G(d)	B3LYP/ 6-311++G(3df,3pd)
CH_3OCH_3	−0.919	−0.932	−0.921
CH_3OCF_3	−0.978	−0.980	−0.979
CHF_2OCHF_2	−0.741	−0.987	−0.742
CHF_2OCF_3	−0.886	−0.890	−0.888

TABLE 4: Rotational Barriers of the Methyl Hydrogens[a]

species	B3LYP/ 6-311++G(3df,3pd)	expt
CH_3OCH_3	2.4	2.60
CH_3OCF_3	1.1	
CHF_2OCHF_2	3.6	
CHF_2OCF_3	2.9	

[a] Barriers are in units of kcal mol^{-1}.

If bonding between hydrogen and fluorine were present, the H−F distance in E143a would be shorter than the H−H distance in dimethyl ether.

The effect of the CF_3 electron-withdrawing group is manifested in C−O distances. The C−O bond adjacent to the CF_3 group decreases in length from 1.410 Å in dimethyl ether to 1.337 Å in E143a, while the opposing C−O bond distance increases from 1.410 to 1.439 Å. The C−H bond lengths in CH_3OCF_3 also decrease. This decrease in bond length may result in a stronger C−H bond, which may contribute to the sharp decrease in reaction rate with hydroxyl radical as compared to dimethyl ether.

Unlike the previous two eclipsed structures, the geometry of CHF_2OCHF_2 (E134) is more staggered. The molecule takes this conformation in an attempt to minimize repulsions between fluorine atoms. E134 is close to C_s symmetry, with dihedrals of 10.4° and 179.2°. However, when this molecule is constrained to C_s symmetry, a negative frequency is obtained, indicating that the symmetric conformation is not the lowest energy structure.

E143a has a large electron-withdrawing group at one end of the molecule, and as a result the two C−O distances differ markedly in length. In E134, however, equivalent functional groups flank both sides of the oxygen atom, so that the two C−O distances differ in length by only 0.02 Å. The COC angle is again slightly larger with the addition of one more fluorine atom.

CHF_2OCF_3 (E125) is very similar to E134 in that it exists as a staggered molecule with dihedrals of 177.3° and 19.5°. E125 belongs to the C_1 symmetry group, with its only hydrogen in an axial site, oriented in a rather shielded position. The COC angle continues to increase as fluorine atoms replace hydrogen. The two C−O distances differ by roughly 0.035 Å, with the C−O distance adjacent to the CF_3 group being the shorter of the two.

B. Rotational Analysis of Fluorinated Ethers. *1. Rotational Structure.* Rotational constants for dimethyl ether as calculated at various levels of theory are displayed in Table 2 along with experimental values obtained from microwave studies by Myers et al. and Neustock et al.[11] Both theoretical methods show reasonable agreement with experimental values, with MP2 values having an error of not more than 0.5% and B3LYP having an error of not more than 2.2%.

Dimethyl ether is an asymmetric top molecule with an asymmetry parameter of −0.92, as shown in Table 3, making it a near-prolate top with a rotational spacing of $2B = 20226$ GHz. Transitions consistent with *b type* selection rules should

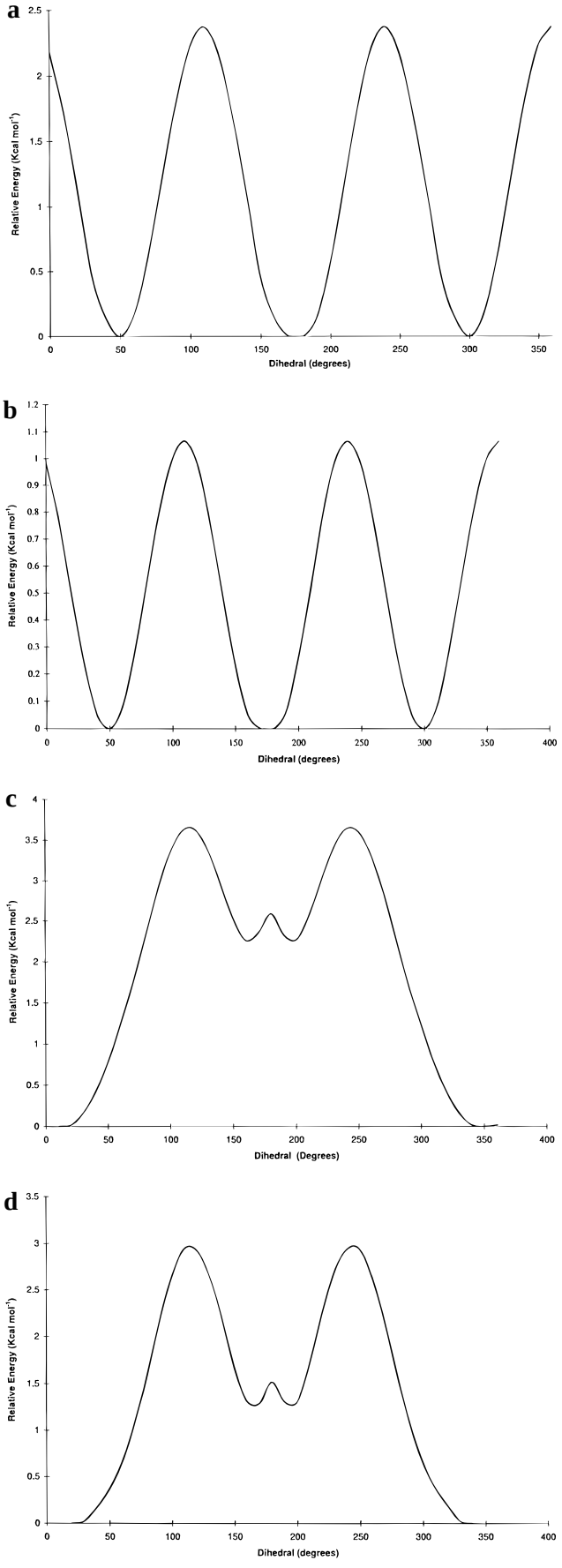

Figure 2. Rotational potential energy surface for dimethyl and fluorinated ethers: (a) CH_3OCH_3, (b) CH_3OCF_3, (c) CHF_2OCHF_2, and (d) CHF_2OCF_3.

TABLE 5: Comparison of Calculated and Experimental Vibrational[a] Frequencies and Assignments for Dimethyl Ether

			MP2/6-31G(d)		QCISD/6-31G(d)		B3LYP/ 6-311++G(3df,3pd)		experiment[b]	
mode symmetry	mode number	description	frequency	absolute intensity	frequency	absolute intensity	frequency	absolute intensity	frequency	relative intensity
A_1	ν_1	sym CH stretch	3218	26	3163	30	3113	20	2993	M
	ν_2	sym CH_2 stretch	3059	48	3020	51	2974	67	2822	M
	ν_3	sym HCH_2 bend	1582	0.3	1567	0.3	1513	4	1470	W
	ν_4	sym HCH bend	1546	0	1534	0	1488	0	1454	W
	ν_5	methyl rock	1300	4	1297	5	1267	6	1250	W
	ν_6	sym CO stretch	974	34	973	33	937	37	918	M
	ν_7	COC bend	428	3	429	3	410	3	424	W
A_2	ν_8	asym CH_2 stretch	3123	0	3069	0	3013	0	2893	W
	ν_9	asym HCH bend	1547	0	1531	0	1483	0	1444	W
	ν_{10}	methyl rock	1195	0	1185	0	1162	0	1150	W
	ν_{11}	methyl torsion	222	0	217	0	205	0	198	W
B_1	ν_{12}	asym CH_2 stretch	3117	126	3066	138	3008	128	2989	S
	ν_{13}	sym HCH bend	1558	10	1542	9	1491	14	1462	M
	ν_{14}	methyl rock	1230	6	1223	7	1193	7	1181	W
	ν_{15}	methyl torsion	269	7	265	7	236	5	242 (236)	W
B_2	ν_{16}	asym CH stretch	3217	26	3161	33	3114	30	2991	M
	ν_{17}	sym CH_2 stretch	3051	46	3009	46	2963	60	2820	M
	ν_{18}	asym HCH bend	1565	12	1549	12	1496	12	1456	W
	ν_{19}	asym HCH bend	1511	9	1500	10	1461	2	1449	W
	ν_{20}	methyl rock	1239	104	1207	110	1194	96	1165	S
	ν_{21}	asym CO stretch	1155	27	1147	22	1117	51	1092	M

[a] Frequencies expressed in cm^{-1} and intensities in km mol^{-1}. [b] Snyder, R. G.; Zerbi, G. *Spectrochim. Acta* **1967**, *23A*, 391.

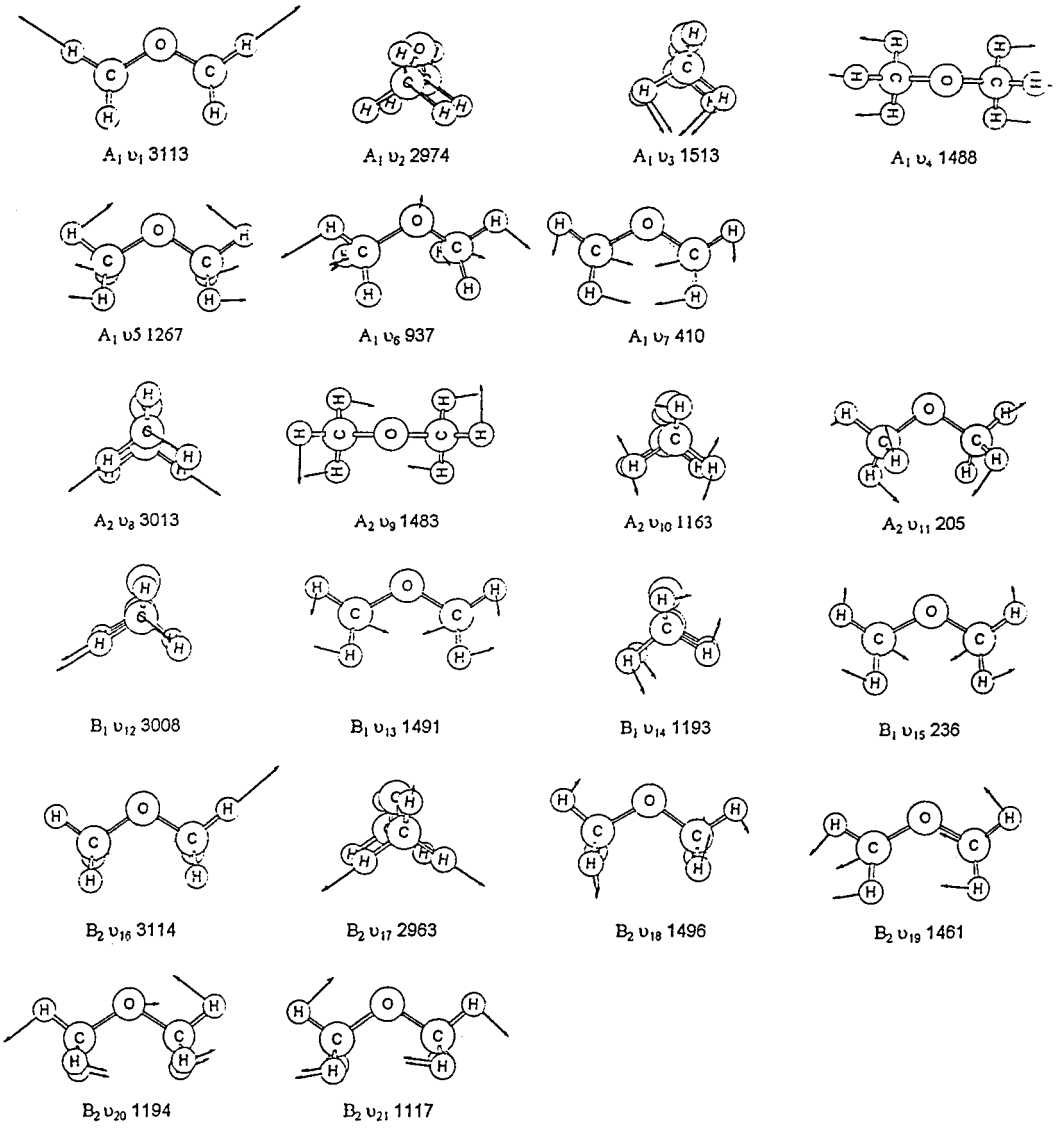

Figure 3. Vector projections of the vibrational fundamental modes of CH_3OCH_3.

TABLE 6: Comparison of Calculated Vibrational Frequencies (cm^{-1}) and Absolute Intensities (km mol^{-1}) with the Experimental Frequencies for CH_3OCF_3 (E143a)

			B3LYP/6-311++G(3df,3pd)		experiment	
mode symmetry	mode number	description	frequency	absolute intensity	frequency	relative intensity
A′	ν_1	CH stretch	3165	7	2984	W
	ν_2	CH_3 sym stretch	3053	26	2880	W
	ν_3	sym HCH bend	1507	16		
	ν_4	CH_3 umbrella	1490	28	1464	M
	ν_5	CF stretch	1278	575	1264	S
	ν_6	methyl rock	1244	129	1248	S
	ν_7	CF_2 sym stretch	1168	200	1160	S
	ν_8	CO asym stretch	1071	32	1064	M
	ν_9	CO sym stretch	839	11	840	W
	ν_{10}	CF_3 rock	655	2		
	ν_{11}	sym CF_2 bend	581	8		
	ν_{12}	FCF bend	441	5		
	ν_{13}	COC bend	262	5		
A″	ν_{14}	CH_2 asym stretch	3127	13	3024	W
	ν_{15}	asym HCH bend	1498	5	1464	M
	ν_{16}	methyl rock	1181	0.1		
	ν_{17}	CF_2 asym stretch	1121	362		
	ν_{18}	asym CF_2 bend	611	3		
	ν_{19}	CF_3 rock	429	0.2		
	ν_{20}	CH_3 methyl torsion	159	3		
	ν_{21}	CF_3 methyl torsion	87	2		

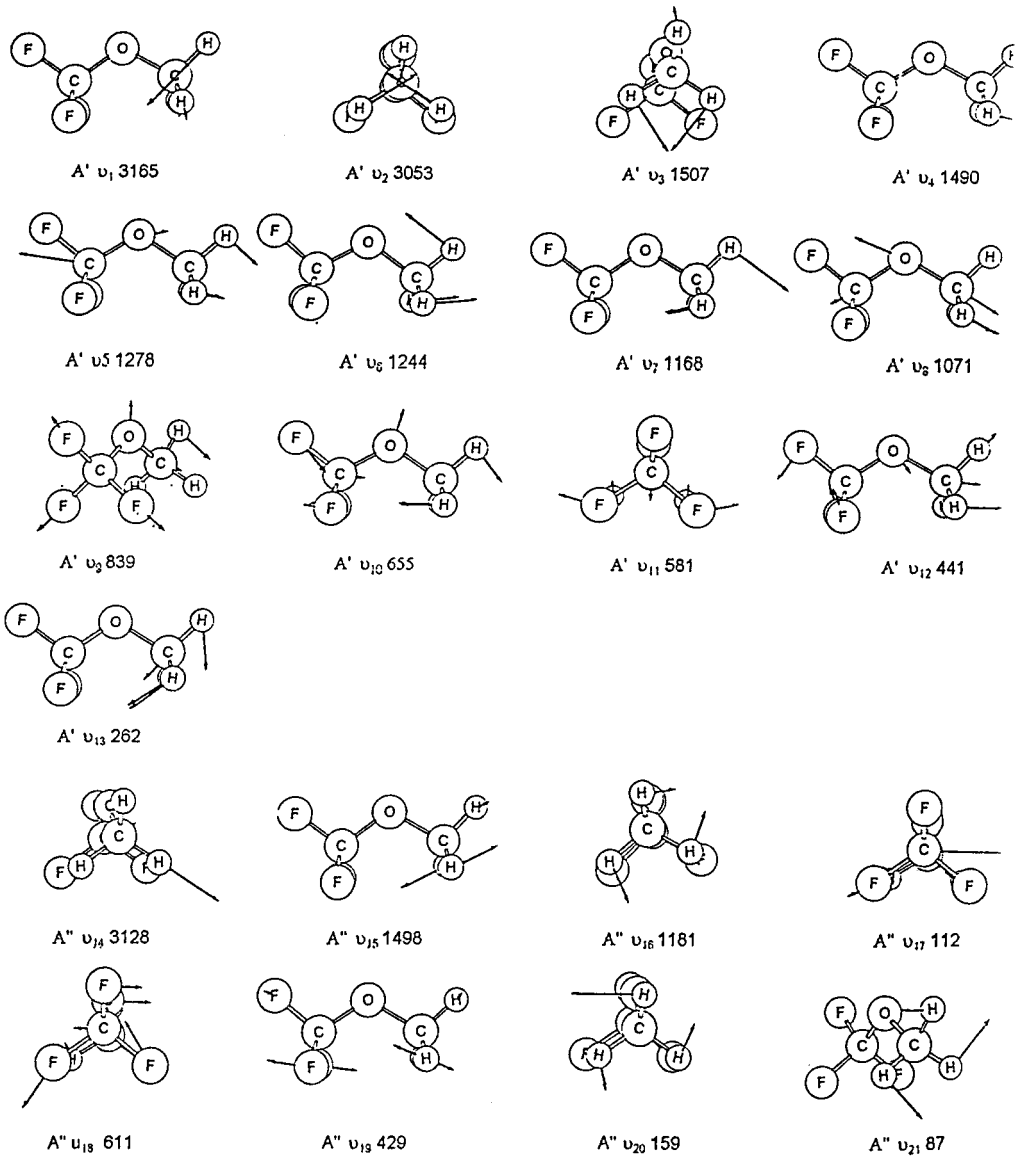

Figure 4. Vector projections of the vibrational fundamental modes of CH_3OCF_3 (E143a).

TABLE 7: Comparison of Calculated Vibrational Frequencies (cm^{-1}) and Absolute Intensities (km mol^{-1}) with the Experimental Frequencies for CHF_2OCHF_2 (E134)

			B3LYP/6-311++G(3df,3pd)		experiment	
mode symmetry	mode number	description	frequency	absolute intensity	frequency	relative intensity
A	ν_1	CH stretch	3154	16	3048	W
	ν_2	CH stretch	3130	12		
	ν_3	asym OCH bend	1430	20	1416	M
	ν_4	sym OCH bend	1404	27		
	ν_5	asym FCH bend	1369	11	1376	W
	ν_6	sym FCH bend	1358	29	1352	M
	ν_7	CO asym stretch	1204	116	1192	S
	ν_8	CF_2 stretch	1141	478		
	ν_9	CF_2 stretch (in phase)	1121	173	1152	S
	ν_{10}	asym $CF_{2'}$ stretch	1115	405		
	ν_{11}	asym $CF_{2'}$ stretch	1054	136	1088	S
	ν_{12}	CO sym stretch	991	169	1000	S
	ν_{13}	CF_2 rock	783	40	776	W
	ν_{14}	asym FCF bend	626	3		
	ν_{15}	sym CF_2 wag (rock)	575	2		
	ν_{16}	sym FCF bend	525	10		
	ν_{17}	$CF_{2'}$ rock	450	8		
	ν_{18}	asym CF_2 wag (rock)	397	0.2		
	ν_{19}	COC bend	203	3		
	ν_{20}	methyl torsion	81	2		
	ν_{21}	methyl torsion	24	2		

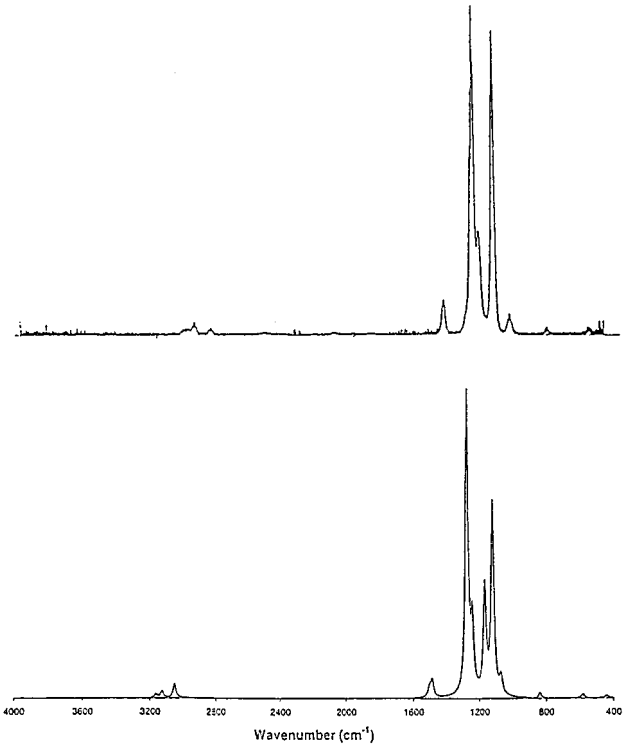

Figure 5. (a) Experimental infrared spectrum for CH_3OCF_3. (b) Simulated infrared spectrum for CH_3OCF_3 from ab initio calculations.

apply to dimethyl ether. The fluorinated ethers are also asymmetric, near-prolate tops. The *B* rotational constants listed in Table 2 suggest successive decreases in rotational splitting with substitution of relatively light hydrogen atoms for fluorine atoms. CH_3OCF_3 (E143a), like dimethyl ether, should display *b type* selection rules, while CHF_2OCHF_2 (E134) and CHF_2OCF_3 (E125) should display *c type* selection rules. E134 and E125 show substantial deviations from the prolate top value of −1.0, with E134 having the highest asymmetry parameter of −0.74.

2. Rotational Barriers for Methyl Hydrogens on Fluorinated Ethers. The rotational barriers for each ether are illustrated in Figure 2 and tabulated in Table 4. Dimethyl ether and CH_3OCF_3 both have methyl groups of 3-fold rotational symmetry. Thus, for both molecules an energy minimum is reached at every 120° rotation of the methyl group and an energy maximum at every 60° rotation. The barrier height for dimethyl ether is 2.4 kcal mol^{-1}, well within 7.7% of the values derived from rotational analysis.[12] The torsional mode for dimethyl ether lies at 0.67 kcal mol^{-1} (236 cm^{-1}) at 298 K. In addition, the rate of tunneling through the barrier is insignificant.[12] Thus, four equivalent equatorial hydrogen environments and two equivalent axial hydrogen environments combine to yield two distinct reactive sites.

CH_3OCF_3 has a rotational barrier of 1.1 kcal mol^{-1}, with its torsional mode at 0.45 kcal mol^{-1}. The difference in barrier height between dimethyl ether and E143a can be rationalized by examining the structural differences between the two molecules. In dimethyl ether, the C−O bond length is 1.410 Å, while the CH_3−O bond length in E143a is 1.440 Å. (In fact, the C−O bond in E143a is longer than any other C−O bond in any other ether.) The CH_3 group in E143a is oriented farthest away from the rest of the molecule, thus minimizing interactions between the CH_3 group and the rest of the molecule, which results in a lower barrier to internal rotation than dimethyl ether.

CHF_2OCHF_2 has a barrier to internal rotation of over 3.6 kcal mol^{-1} and a torsional mode of only 0.23 kcal mol^{-1}. Therefore, E134 is unlikely to undergo significant internal rotation, thus yielding two distinct hydrogen environments. One hydrogen atom is oriented upward and away from the oxygen center. The second hydrogen atom is oriented downward and toward the oxygen center in a more shielded environment.

CHF_2OCF_3 also has a relatively high barrier to internal rotation of 2.9 kcal mol^{-1}. Its torsional mode lies at 0.17 kcal mol^{-1}, leaving the only hydrogen oriented downward in a shielded environment.

C. Vibrational Analysis of Fluorinated Ethers. *1. Calibration of Methods for Vibrational Analysis of Fluorinated Ethers: CH_3OCH_3 as Calibrant.* To determine the reliability of the various methods for predicting the vibrational frequencies for the fluorinated ethers, we selected dimethyl ether as a calibrant since the fundamental vibrational modes are experi-

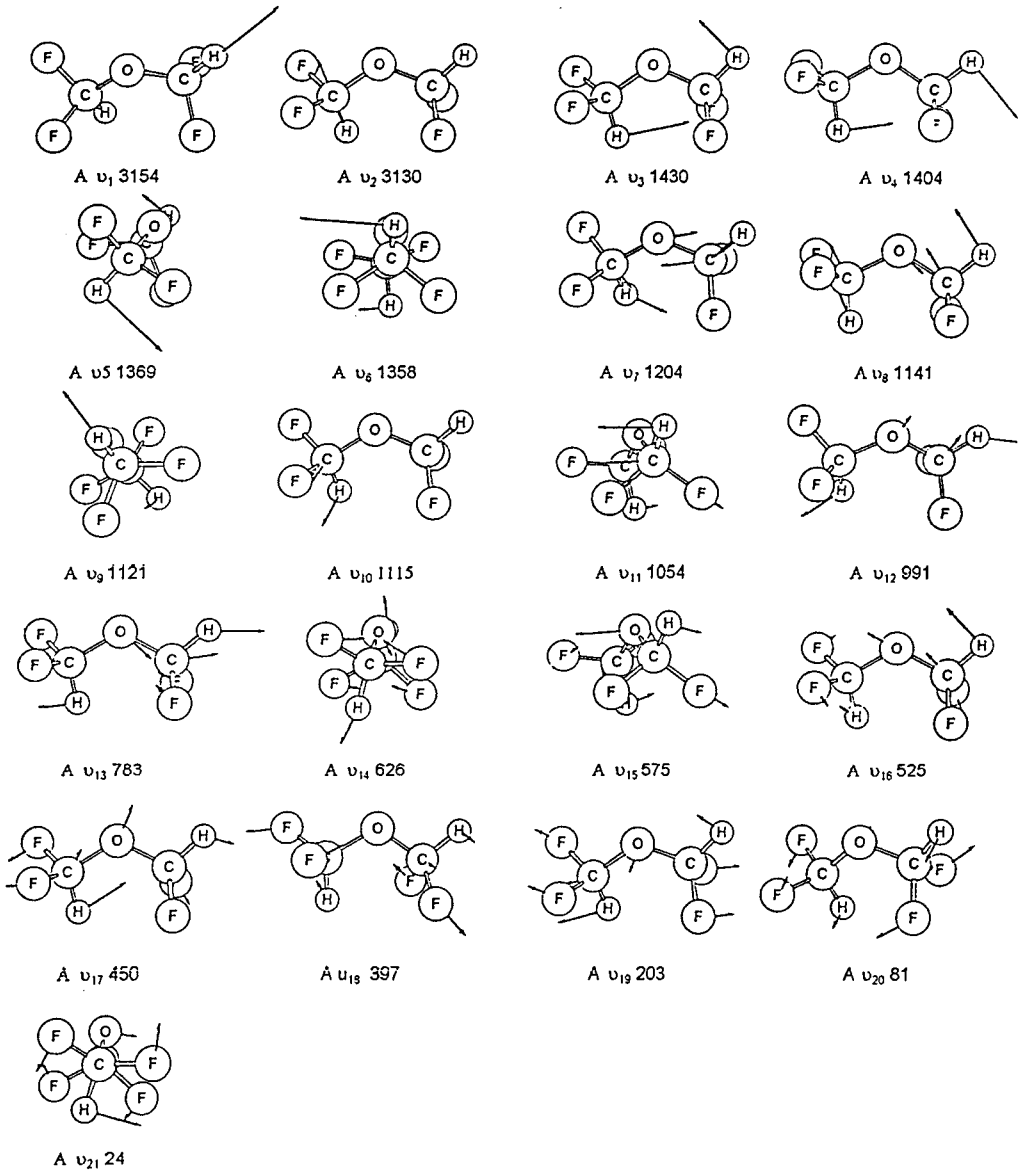

Figure 6. Vector projections of the vibrational fundamental modes of CHF_2OCHF_2 (E134).

TABLE 8: Comparison of Calculated Vibrational Frequencies (cm^{-1}) and Absolute Intensities (km mol^{-1}) with the Experimental Frequencies for CHF_2OCF_3 (E125)

			B3LYP/6-311++G(3df,3pd)		experiment	
mode symmetry	mode number	description	frequency	absolute intensity	frequency	relative intensity
A	ν_1	CH stretch	3120	14	3032	W
	ν_2	OCH stretch	1424	7	1400	W
	ν_3	FCH bend	1372	31	1364	M
	ν_4	CF sym stretch	1287	381	1288	S
	ν_5	CF_2 sym stretch	1222	367	1238	S
	ν_6	CF_2 asym stretch	1166	514		
	ν_7	$CF_{2'}$ sym stretch	1146	287	1152	S
	ν_8	$CF_{2'}$ asym stretch	1114	68	1110	M
	ν_9	CO asym stretch	1089	315	1110	S
	ν_{10}	CO sym stretch	907	104	909	S
	ν_{11}	CF_3 asym rock	721	14	718	M
	ν_{12}	sym rock	645	5		
	ν_{13}	FCF bend	617	3		
	ν_{14}	FCF bend	586	10	584	W
	ν_{15}	FCF bend	513	2		
	ν_{16}	FCF bend	462	5		
	ν_{17}	asym wag	371	0.5		
	ν_{18}	sym wag	355	0		
	ν_{19}	COC bend	188	3		
	ν_{20}	torsion	60	0.1		
	ν_{21}	torsion	24	1		

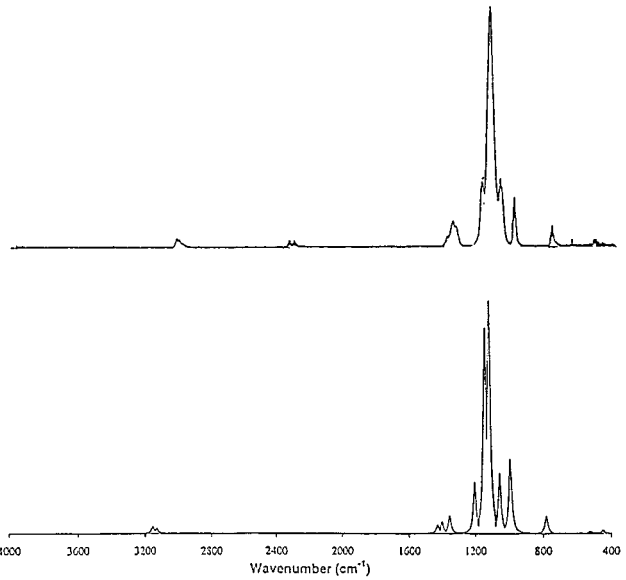

Figure 7. (a) Experimental infrared spectrum for CHF_2OCHF_2. (b) Simulated infrared spectrum for CHF_2OCHF_2 from ab initio calculations.

mentally well characterized. Frequency assignments for dimethyl ether as calculated at the various levels of theory are shown in Table 5, along with experimental values taken from the work of Snyder et al. for comparison.[13] The structural model used to describe dimethyl ether assumed C_{2v} symmetry. This divides the 21 normal vibrational modes into the following vibrational representation:

$$\Gamma_{vib} = 7A_1 + 4A_2 + 6B_1 + 4B_2$$

The A_2 transitions are forbidden and not observed in the infrared. The two lowest energy vibrations are the CH_3O methyl torsions at 198 and 242 cm^{-1}. There are eight stretching modes, six of which are CH type stretches: a symmetric [2993 cm^{-1} (A_1)] and an asymmetric [2991 cm^{-1} (B_1)] mode involving the two axial hydrogens; four CH_2 stretching modes involving the four equatorial hydrogens; two symmetric stretches [2822 cm^{-1} (A_1) and 2820 cm^{-1} (B_1)]; and two asymmetric stretches [2893 cm^{-1} (A_2) and 2989 cm^{-1} (B_1)]. The remaining two stretches are the symmetric (918 cm^{-1}) and asymmetric (1092 cm^{-1}) C−O stretches of the ether linkage.

There are 11 bending modes, four of which are methyl rocking modes (1250, 1181, 1165, and 1150 cm^{-1}). The COC bend occurs at 424 cm^{-1}, leaving the six HCH bends. These HCH bends include three symmetric and three asymmetric modes. Modes ν_{18} (B_2) at 1456 cm^{-1} and ν_3 (A_1) at 1470 cm^{-1} correspond to the vibrational motions of the four equatorial hydrogens, while the remaining four modes describe the in-plane and out-of-plane axial hydrogen motions. The mode descriptions for dimethyl ether are consistent with the experimental interpretation. The vector projections of all 21 fundamental modes of dimethyl ether are illustrated in Figure 3.

Usually vibrational frequencies calculated at the MP2/6-31G(d) level are found to overestimate experimental anharmonic frequencies by 5−10%, so a popular approach has been to use scale factors.[14] However, in the procedure adopted in this work no scaling factors are applied. A comparison of observed and calculated frequencies for dimethyl ether shows that the results at the MP2/6-31G(d) level of theory are within 6.6% (rms) of experiment and those at the QCISD/6-31G(d) level are within 5.4% (rms error) of the experimental anharmonic frequencies. Only marginal improvement is achieved with the QCISD level. Substantial improvement is, however, obtained using the B3LYP level of theory with the 6-311++G(3df,3pd) basis set. A rms error of only 2.7% is achieved.

2. CH_3OCF_3 (E143a). The structural model used to describe CH_3OCF_3 (E143a) assumed C_s symmetry. The 21 normal vibration modes were divided into 13 modes of the A′ representation and eight modes of the A″ type, i.e.

$$\Gamma_{vib} = 13A' + 8A''$$

All 21 fundamental modes are allowed and active in both the infrared and Raman. The A′ species are symmetric and the A″ species are antisymmetric to the plane of the molecule. Experimental and theoretical frequencies, along with assignments, are presented in Table 6, while vector projections of all modes are illustrated in Figure 4. The two torsional modes are weak bands located at 87 and 159 cm^{-1}. They correspond to a CF_3 torsion and a CH_3 torsion, respectively. The eight stretching modes consist of three CH stretches, three CF stretches, and two CO stretches. The symmetric CO stretch is shifted down to 839 cm^{-1} compared to the 937 cm^{-1} of dimethyl ether, while the asymmetric CO stretch is shifted from 1117 cm^{-1} in dimethyl ether to 1071 cm^{-1}. The three CH stretching modes appear in the usual CH stretching region: a symmetric CH_3 stretching mode at 3053 cm^{-1}, an asymmetric CH_2 mode at 3127 cm^{-1}, and a CH mode at 3165 cm^{-1}. All three of these modes are relatively weak in contrast to dimethyl ether. The three C−F stretches resonate at 1278 cm^{-1} (CF stretch, axial fluorine), 1168 cm^{-1} (CF_2 symmetric stretch of equatorial fluorines), and 1121 cm^{-1} (CF_2 asymmetric stretch equatorial fluorines). The stretching mode at 1168 cm^{-1} contains substantial methyl rocking character just as the methyl rocking mode at 1244 cm^{-1} contains significant CF_2 stretching character. Such mode mixing makes unambiguous assignment difficult. The CF stretching modes are very intense modes that dominate the spectra. The only exception to this is the aforementioned methyl rocking mode at 1244 cm^{-1}, which has significant CF stretching character. The 11 bends for CH_3OCF_3 consist of one COC mode, three HCH bending modes, three FCF modes, and four rocking modes. The three CH modes consist of a CH_3 umbrella at 1490 cm^{-1}, a symmetric HCH bend at 1507 cm^{-1}, and an asymmetric stretch at 1498 cm^{-1}. These modes are once again relatively weak. The three CF bending modes consist of an FCF mode, which involves predominately the axial fluorine (441 cm^{-1}), and two modes involving the two equatorial fluorines: a symmetric bend at 581 cm^{-1} and an asymmetric bend at 611 cm^{-1}. Finally, the four rocking modes are broken down into two methyl rocks (1244 and 1181 cm^{-1}) and two CF_3 rocks (655 and 429 cm^{-1}).

The rms error between calculated and observed frequencies is quite reasonable: 3.2%. As a further test of the reliability of the calculations, we simulated the infrared spectra from the ab initio frequencies. The simulated spectra were generated using the calculated frequencies as the mean of a Lorentzian distribution with a full width at half-maximum (fwhm) of 16 cm^{-1}. The Lorentzian is given by the following expression:

$$\frac{1}{\pi}\frac{\Delta x/2}{(\Delta x/2)^2 + (x-u)^2} \qquad (1)$$

where u is the mean or central frequency and Δx is the fwhm. The simulated and experimental spectra for CH_3OCF_3 (E143a) are illustrated in parts a and b of Figure 5, respectively. The simulated spectrum (Figure 5a) shows reasonable agreement

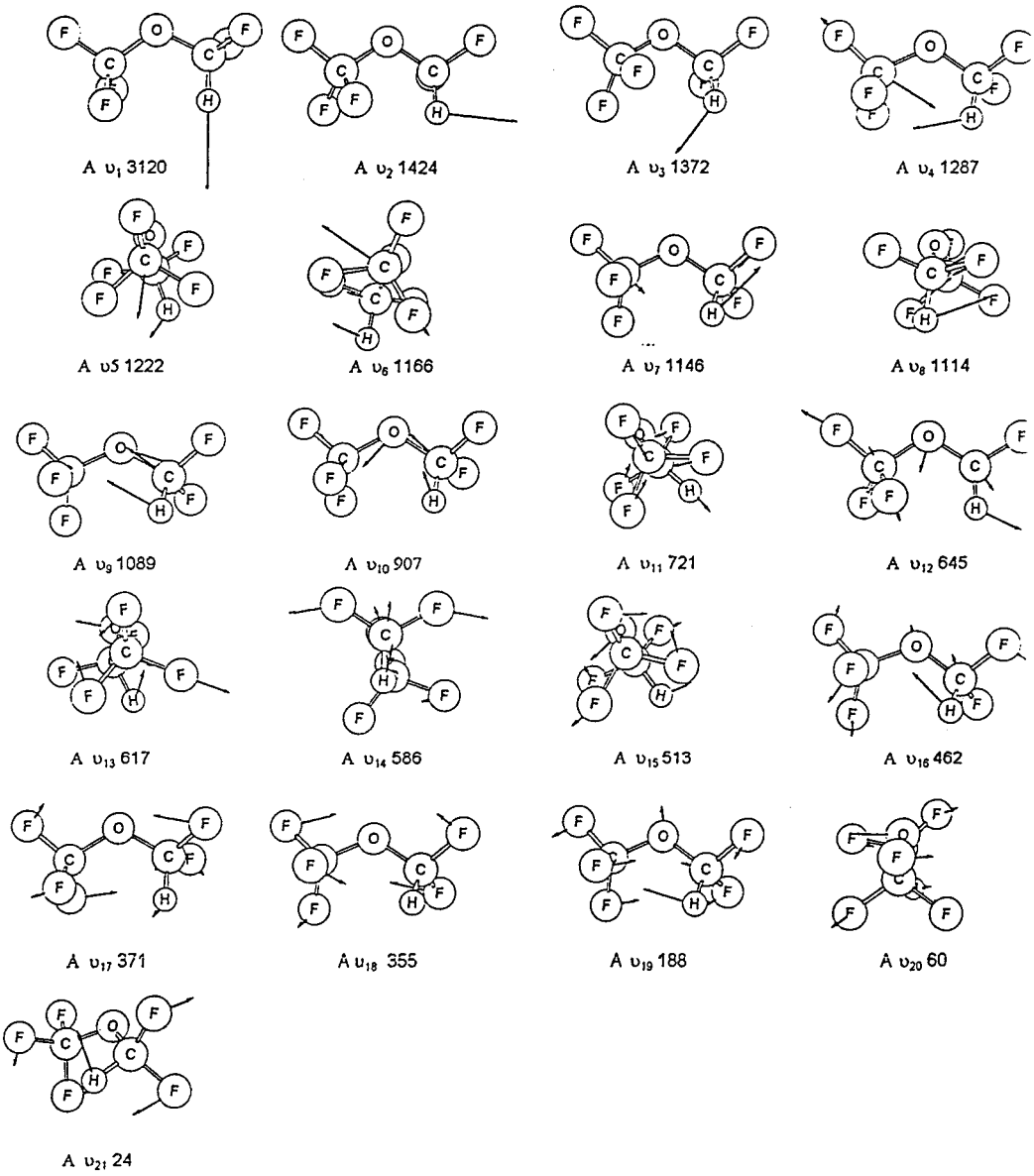

Figure 8. Vector projections of the vibrational fundamental modes of CHF_2OCF_3 (E125).

with the experimental spectrum (Figure 5b). The experimental peak at 1160 cm^{-1} is composed of two unresolved CF_2 stretching modes, which are shown in the simulated spectrum at 1121 cm^{-1} and 1168 cm^{-1}. The band at 1260 cm^{-1} in the experimental spectrum is a convolution of the CF stretch and methyl rock, shown in the simulated spectrum at 1278 cm^{-1} and 1244 cm^{-1}, respectively. The cluster of modes centered around 1465 cm^{-1} is the HCH bending modes, while the cluster around the 3100 cm^{-1} region is the CH stretching modes.

3. CHF_2OCHF_2 (E134). CHF_2OCHF_2 (E134) belongs to the C_1 point group, in which all of the 21 normal modes are allowed. Frequencies and their assignments are listed in Table 7, while vector projections are displayed in Figure 6. E134 again displays the same number of torsions, stretches, and bends as the previous two examples. The torsional modes are lower in energy (24 and 81 cm^{-1}) relative to the torsional modes in dimethyl ether (222 and 269 cm^{-1}). The symmetric and asymmetric CO stretching modes lie at 991 and 1204 cm^{-1}. There are two CH stretching modes at 3154 and 3130 cm^{-1}. The 3154 cm^{-1} mode is the asymmetric stretch, with motion dominated by the outwardly oriented hydrogen. The 3130 cm^{-1} mode is the symmetric stretch, with motion dominated by the inwardly oriented hydrogen. The four CF stretching modes consist of the following: (1) two modes in which the individual fluorine atoms on opposite sides of the oxygen atom move in-phase, with both a symmetric (1121 cm^{-1}) and an asymmetric (1115 cm^{-1}) mode; (2) two modes in which the individual fluorine atoms on opposite sides of the oxygen atom move out-of-phase, with a symmetric (1141 cm^{-1}) and an asymmetric (1054 cm^{-1}) mode.

The 11 bending motions consist of four rocks, two FCF bends, two OCH bends, two HCF bends, and a COC bend. The two modes at 1430 and 1404 cm^{-1} correspond to the two OCH bending modes: an in-phase and an out-of phase mode, respectively. The two vibrations at 1369 and 1358 cm^{-1} describe the motion of the hydrogen atoms in a plane nearly perpendicular to the COC plane, which allows mixing of motion from the HCF angle. The mode at 1369 cm^{-1} is the out-of-phase bend, while the 1358 cm^{-1} mode is the in-phase bend. The two FCF type bends occur at 525 cm^{-1} (out-of-phase) and at 626 cm^{-1}(in-phase). The remaining four bending modes are the rocking modes at 397, 450, 575, and 783 cm^{-1}.

The simulated spectrum in Figure 7a can be compared to the experimental spectrum in Figure 7b. The experimental peak at

776 cm^{-1} corresponds to the CF_2 rocking mode at 783 cm^{-1} in the simulated spectrum. The peak at 1000 cm^{-1} is the CO symmetric stretch, calculated at 991 cm^{-1}. The main peak of the experimental spectrum may appear to consist of three unresolved peaks when in fact it consists of five. Only four of the five are observable in the simulated spectrum with this line width. The first relatively medium strength peak (168 km mol^{-1}) at 1088 cm^{-1} corresponds to a CF_2 stretching mode, calculated at 1054 cm^{-1}. The largest peak in the spectrum is centered at 1152 cm^{-1} and is actually a convolution of three CF_2 stretching modes. One relatively weak mode (173 km mol^{-1}) at 1121 cm^{-1} is sandwiched between two very intense modes (405 and 478 km mol^{-1}) at 1115 and 1141 cm^{-1}. The next experimentally observable peak at 1192 cm^{-1} is the CO asymmetric mode, simulated at 1204 cm^{-1}. The cluster of peaks at 1352, 1376, and 1416 cm^{-1} is the CH bending modes described previously at 1358, 1369, 1404, and 1430 cm^{-1}. The final cluster at 3048 cm^{-1} in the experimental spectrum is the CH stretches calculated at 3130 and 3154 cm^{-1}. The simulated and experimental spectra are in reasonable agreement. Moreover, the rms error between calculated and observed frequencies is 1.6% for CHF_2OCHF_2.

4. CHF_2OCF_3 (E125). The 21 allowed normal modes for CHF_2OCF_3 are listed in Table 8. Vector projections are illustrated in Figure 8. The two torsional modes lie at 24 and 60 cm^{-1}, followed by the COC bend at 188 cm^{-1}. Of the eight stretches, there are five CF stretches, two CO stretches, and a CH stretch. The CH stretch is located at 3120 cm^{-1}, while the asymmetric and symmetric CO stretches lie at 1089 and 907 cm^{-1}, respectively. The five CF stretching modes consist of a CF stretch at 1287 cm^{-1} and four stretches of the CF_2 type. The 10 remaining bending modes consist of a OCH bend at 1424 cm^{-1} and an FCH bend at 1372 cm^{-1}. The four FCF bending modes are located between 462 and 617 cm^{-1}, while the four rocking modes consist of two wagging modes at 355 cm^{-1} (in-phase) and 371 cm^{-1} (out of phase) and two rocking modes at 645 and 721 cm^{-1}.

The simulated spectrum is displayed in Figure 9a, while the experimental spectrum is illustrated in Figure 9b. The experimental peak at 718 cm^{-1} is the CF_3 rocking motion simulated at 721 cm^{-1}. The next peak at 909 cm^{-1} is the symmetric CO stretching mode calculated to be around 907 cm^{-1}. The next large cluster of peaks centered around 1200 cm^{-1} appears to be a convolution of four peaks, but actually consists of six peaks. The first peak is the relatively intense CO asymmetric stretching mode (315 km mol^{-1}) at 1110.4 cm^{-1} (experimental) or 1089.4 cm^{-1} (theoretical). The next low-intensity peak (68 km mol^{-1}) is completely unresolved in the experimental spectrum and only barely visible in the simulated spectrum. The peak at 1152 cm^{-1} is shown resolved in the experimental spectrum. In the simulated spectrum, however, it is nearly convolved with the 1166 cm^{-1} peak. The simulated spectrum convolutes ν_6 and ν_7, while the experimental spectrum shows ν_5 and ν_6 as being convolved. The ν_6 mode, a CF_2 asymmetric stretch, is the most intense peak with a band strength of over 500 km mol^{-1}. The sixth peak in the cluster, ν_4, is shown resolved in both spectra and corresponds to the CF stretching mode at 1288 cm^{-1} (1287 cm^{-1} experimentally). The two remaining regions of the spectrum are the hydrogen bending modes around 1400 cm^{-1} and the hydrogen stretching modes at 3032 cm^{-1}.

D. Atmospheric Implications. Below 800 cm^{-1} water in the atmosphere absorbs thermal radiation, while above 1400 cm^{-1} water and carbon dioxide both absorb. Thus there exists a region between 800 and 1400 cm^{-1} where thermal radiation emitted from Earth can escape. It is therefore expected that halons with absorption features in this area could contribute to global warming depending on the strength of their absorption features. Dimethyl ether has a majority of its spectral features outside the thermal window. Only the methyl rock and the two CO stretches contribute significantly to absorption in the specified window region. This corresponds to a total band strength of approximately 147.2 km mol^{-1}(see Table 5).

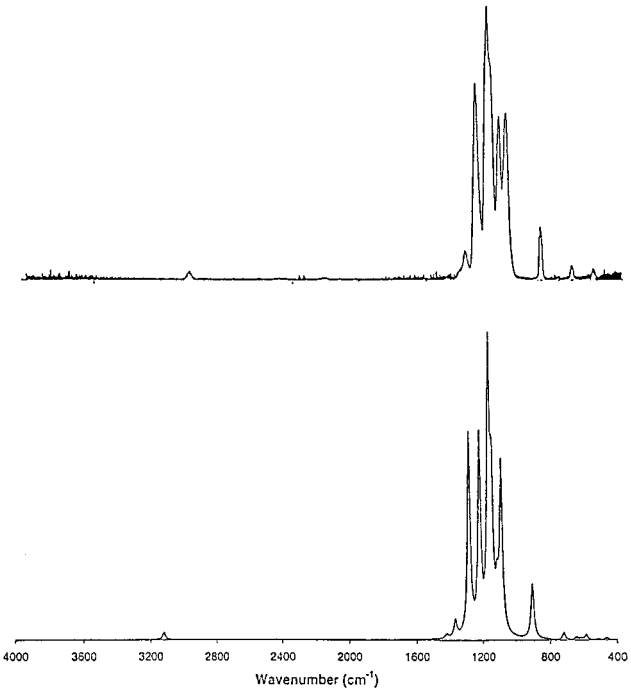

Figure 9. (a) Experimental infrared spectrum for CHF_2OCF_3. (b) Simulated infrared spectrum for CHF_2OCF_3 from ab initio calculations.

The result of fluorination is to replace CH stretches whose absorption features lie outside of the window region with CF stretches, whose features lie well within the window region. The insertion of an oxygen atom between the two carbon atoms of a fluorinated ethane replaces a C−C stretch with two intense C−O stretches, which resonate within the window region. The total band strength for E143a in the region between 800 and 1400 cm^{-1} is 1310.7 km mol^{-1}, while the total band strength for E134 is 1545 km mol^{-1}. E125 has a band strength of over 2037 km mol^{-1}. Clearly the substitution of hydrogen with fluorine will have a significant impact on the radiative properties of the molecule.

IV. Conclusion

Dimethyl ether has a short atmospheric lifetime and is expected to degrade in the troposphere. Vibrational analysis shows trivial infrared absorption in the window region. Thus, dimethyl ether is unlikely to be a significant greenhouse gas. The successive fluorination of dimethyl ether decreases the reaction rate with hydroxyl radical, which translates into longer atmospheric lifetimes. Therefore, the possibility exists for substantial concentrations of fluorinated ethers to enter the stratosphere and the ozone layer. Successive fluorination also substantially increases the absorption of infrared radiation within the window region. This, in combination with increased atmospheric lifetimes, implies that fluorinated ethers may contribute to global warming. The magnitude of their contribution in relation to existing halons should be investigated.

Acknowledgment. We thank W. B. DeMore for supplying IR spectra for each fluorinated ether and for constructive comments on the manuscript.

References and Notes

(1) Zhang, Z.; Saini, R. D.; Kurylo, M. J.; Huie, R. E. *J. Phys. Chem.* **1992**, *96*, 9301.

(2) Hsu, K. J.; DeMore, W. B. *J. Phys. Chem.* **1995**, *99*, 11141.

(3) Cooper, D. L.; Cunningham, T. P.; Allan, N. L.; McCulloch, A. *Atmos. Environ.* **1992**, *26*, 1331.

(4) Wuebbles, D. J. *Annu. Rev. Energy Environ.* **1995**, *20*, 45.

(5) Frisch, M. J.; Trucks, G. W.; Schlegel, H. B.; Gill, P. M. W.; Johnson, B. G.; Robb, M. A.; Cheeseman, J. R.; Keith, T.; Peterson, G. A.; Montgomery, J. A.; Raghavachari, K.; Al-Laham, M. A.; Zakrzewski, V. G.; Ortiz, J. V.; Foresman, J. B.; Cioslowski, J.; Stefanov, B. B.; Nanayakkara, A.; Challacombe, M.; Peng, C. Y.; Ayala, P. Y.; Chen, W.; Wong, M. W.; Andres, J. L.; Replogle, E. S.; Gomperts, R.; Martin, R. L.; Fox, D. J.; Binkley, J. S.; Defrees, D. J.; Baker, J.; Stewart, J. P.; Head-Gordon, M.; Gonzales, C.; Pople, J. A. *GAUSSIAN 94*, Revision D.2; Gaussian, Inc.: Pittsburgh, PA, 1995.

(6) Moller, C.; Plesset, M. S. *Phys. Rev.* **1934**, *46*, 618.

(7) Pople, J. A.; Head-Gordon, M.; Raghavachari, K. *J. Chem. Phys.* **1987**, 5968.

(8) Lee, C.; Yang, W.; Parr, R. G. *Phys. Rev. B* **1988**, *41*, 785.

(9) Kasai, P. H.; Myers, R. J. *J. Chem. Phys.* **1959**, *30*, 1096.

(10) Blukis, U.; Kasai, P. H.; Myers, R. J. *J. Chem. Phys.* **1963**, *38*, 2753.

(11) Neustock, W.; Guarnieri, A.; Demaison, J.; Wlodarezak, G. *Naturforsch. Z.* **1990**, *45a*, 702.

(12) Lovas, F. J.; Lutz, H.; Dreizler, H. *J. Phys. Chem. Ref. Data* **1979**, *8*, 1051.

(13) Snyder, R. G.; Zerbi, G. *Spectrochim. Acta* **1967**, *23A*, 391.

(14) Pople, J. A.; Scott, A. P.; Wong, M. W.; Radom, L. *Isr. J. Chem.* **1990**, *33*, 345.